# Balanced photoreceivers for analog and digital fiber optic communications

Abhay Joshi, Xinde Wang, Dan Mohr, Don Becker, and Christoph Wree
Discovery Semiconductors, Inc, 119 Silvia Street, Ewing, NJ 08628 USA
Web: http://www.chipsat.com

## ABSTRACT

We have developed 10, 20, 30, and 40 Gb bandwidth balanced photoreceivers which have applications for both analog and digital fiber optic communications. The devices can operate at C and L optical bands as well as 1064 nm and 1310 nm wavelengths. The analog applications include low noise RF photonic links. The digital applications include 10 Gb and 40 Gb DPSK and DQPSK modulation formats for enhanced sensitivities. The advantages of balanced photoreceivers are: RIN noise cancellation, suppression of even order harmonics, doubling the optical power handling capacity of a photonic link, and better reliability.

**Keywords:** InGaAs photodiode, balanced receiver, spurious free dynamic range (SFDR), analog photonic link, Relative Intensity Noise (RIN), and Differential Phase Shift Keying (DPSK).

## 1. INTRODUCTION

Using Wavelength Division Multiplexing (WDM), it is possible to use the same fiber optic backbone for transmission and distribution of both analog and digital signals. To compensate for the losses inherently present in a photonic link, it is desirable to have higher optical power emitted by the laser. However, the Relative Intensity Noise (RIN) of the laser will limit the signal dynamic range of the whole photonic link. The main noises of the photonic link are shot noise and RIN. The RIN detected by the O/E receiver is proportional to the square of the mean photocurrent, whereas the shot noise is linearly proportional to photocurrent. Therefore, the RIN will tend to be the dominant noise, when the laser average power is increasing and will reduce the S/N ratio of the link.

In this paper, we will discuss balanced detection in the analog photonic link by using a balanced receiver that consists of high optical power handling InGaAs photodiodes and measure spurious free dynamic range (SFDR) of the link. Furthermore, we will also demonstrate the use of these balanced photoreceievers for 10 Gb and 40 Gb digital systems using newer modulation formats such as Differential Phase Shift Keying (DPSK) and Differential Quadrature Phase Shift Keying (DQPSK).

## 2. HIGH OPTICAL POWER HANDLING PHOTODIODE

### 2.1 Performance of the photodiode

We have developed 20 mA or higher photocurrent handling InGaAs photodiodes with 20 GHz bandwidth, and 10 mA or higher photocurrent handling InGaAs photodiodes with >40 GHz bandwidth. These photodiodes have been thoroughly tested for reliability including Bellcore GR 468 standard and are built to ISO 9001:2000 Quality Management System. These Dual-depletion InGaAs/InP photodiodes are surface illuminated and yet handle such large photocurrent due to advanced band-gap engineering.

Since 1995, Discovery Semiconductors has pioneered a high-speed detector technology known as the dual-depletion p-i-n photodetector [2]. This design allows good responsivity, high speed, and high saturation currents from a front-illuminated diode that is relatively easy to manufacture and integrate. Figure 1 shows the schematic of Discovery Semiconductors' high speed, high power handling, dual depletion layer InGaAs/InP p-i-n photodetector. They have broad wavelength coverage from 800 nm to 1700 nm, and thus can be used at several wavelengths such as 850 nm, 1064 nm, 1310 nm, 1550 nm, and 1620 nm. Furthermore, they exhibit very low Polarization Dependence Loss (PDL) of 0.05

Enabling Photonics Technologies for Defense, Security, and Aerospace Applications,
edited by A. R. Pirich, M. J. Hayduk, E. J. Donkor, P. J. Delfyett, Jr., Proc. of SPIE Vol. 5814
(SPIE, Bellingham, WA, 2005) · 0277-786X/05/$15 · doi: 10.1117/12.626961

dB typical to 0.1 dB maximum, and very high Optical Return Loss (ORL) of typical 40 dB. The devices are well suited for receiver applications with optical pre-amplification or with laser sources that emit more than 50 mW CW power.

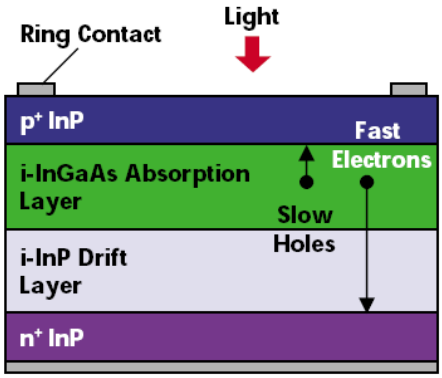


Figure 1. Schematic of Discovery Semiconductors' high speed, high power handling, dual depletion layer InGaAs/InP p-i-n photodetector.

## 3. BALANCED DETECTION

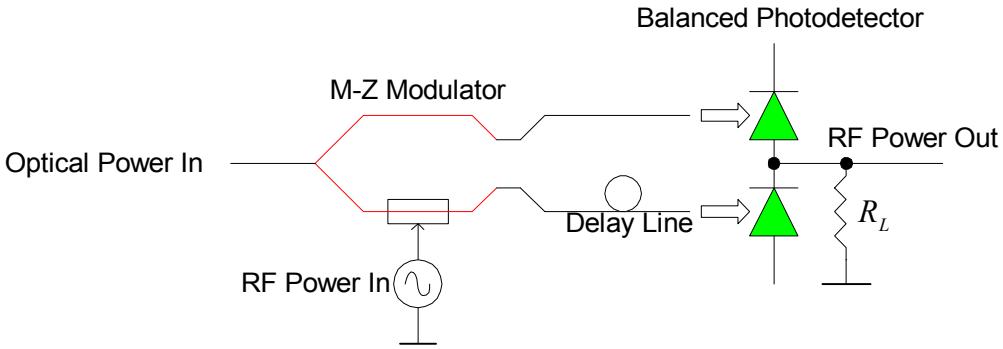


Figure 2. The balanced photodetector can remove the Relative Intensity Noise (RIN) of a laser.

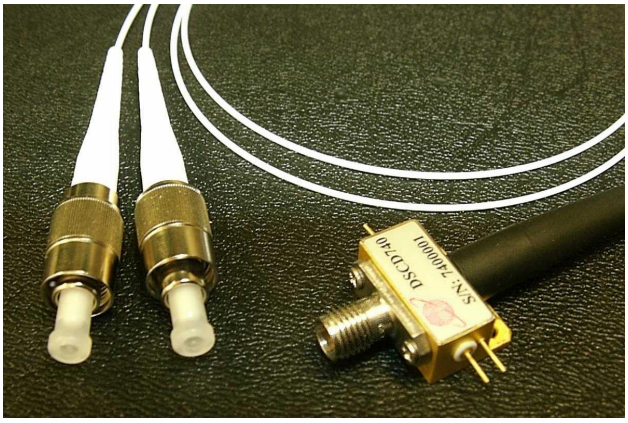

Figure 3. Photograph of the 40 Gb balanced push-pull photodiode. Please note that there are two fiber optic cables for two photodiodes that form a push-pull pair.

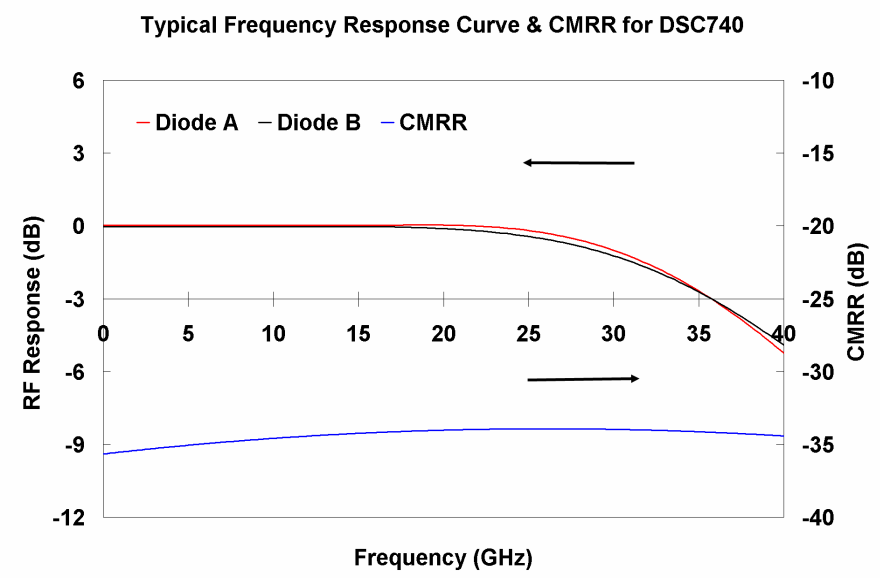


Figure 4. RF response of 40 Gb push-pull balanced photodiode.

The schematic of a balanced photodiode push-pull pair used in an analog link is shown in Figure 2. A differential output modulator produces the needed 180 degrees phase shift between two arms of the push-pull pair. The optical delay line is used to match the path lengths between the two arms of the push-pull pair. Figure 3 shows a photograph of the DSC740 fiber pigtailed module, whereas Figure 4 shows the RF response of Discovery's DSC740 balanced photodiode,.

**3.1 RIN noise cancellation**

There are three dominant noise sources on the optical receiver side of an analog photonic link. Those are thermal, shot, and received relative intensity noise (RIN). The thermal noise is represented by the following equation:

$$\overline{i_{tn}^2} = \frac{4kT_a\Delta f}{R} \tag{1}$$

where, $\overline{i_{tn}^2}$ is the thermal noise mean square current, $T_a$ is the temperature in Kelvin, k is the Boltzmann constant ( $1.38\times10^{-23}\,Joule/K$ ), and $\Delta f$ is the bandwidth of the circuit. The shot noise can be represented by:

$$\overline{i_{sn}^2} = 2e(\overline{I_D} + I_d)\Delta f \tag{2}$$

where, e is the electronic charge, $e = 1.6\times10^{-19}\,Coulomb$, $\overline{I_D}$ is the mean photocurrent, and $I_d$ is the dark current of the photodiode. The Relative Intensity Noise (*RIN*) is the fluctuations of the laser intensity caused by random spontaneous light emissions. The typical values of *RIN* for a distributed feedback (*DFB*) laser are better than -155 dB/Hz [3]. The power spectrum of the *RIN* is not flat, hence it is not a white noise source. In an analog photonic link, we use a photodiode to detect the optical power from the M-Z modulator. Thus, *RIN* can be expressed as:

$$RIN = \frac{\overline{(\frac{i_{RIND}}{\Re})^2}}{\Delta f\,\overline{(\frac{I_D}{\Re})^2}} = \frac{\overline{i_{RIND}^2}}{\Delta f\,\overline{I_D^2}} \tag{3}$$

where, $\Re$ is the current responsivity of the photodetector. From equation (3), we obtain the received mean square current *RIN* noise of the receiver as:

$$\overline{i_{RIND}^2} = RIN \cdot \overline{I_D^2} \Delta f \tag{4}$$

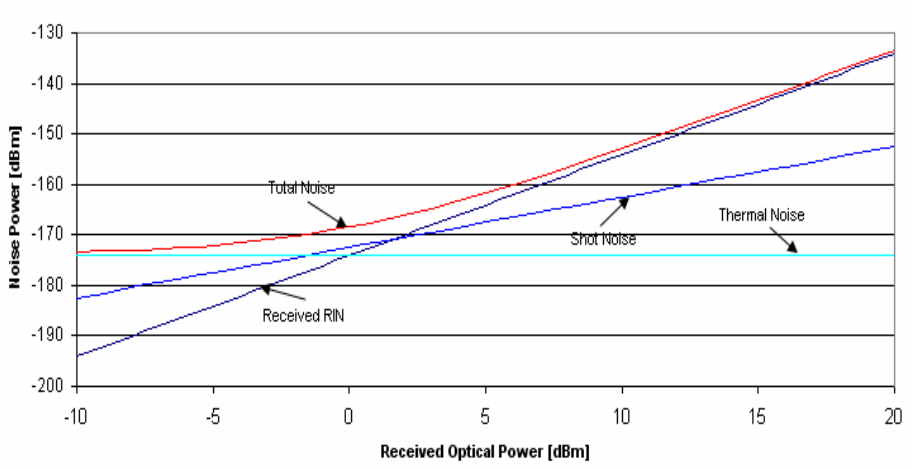


Figure 5. Calculated noise power vs. received optical power of the photodiode, here assuming RIN from the DFB laser is – 155 dB/Hz.

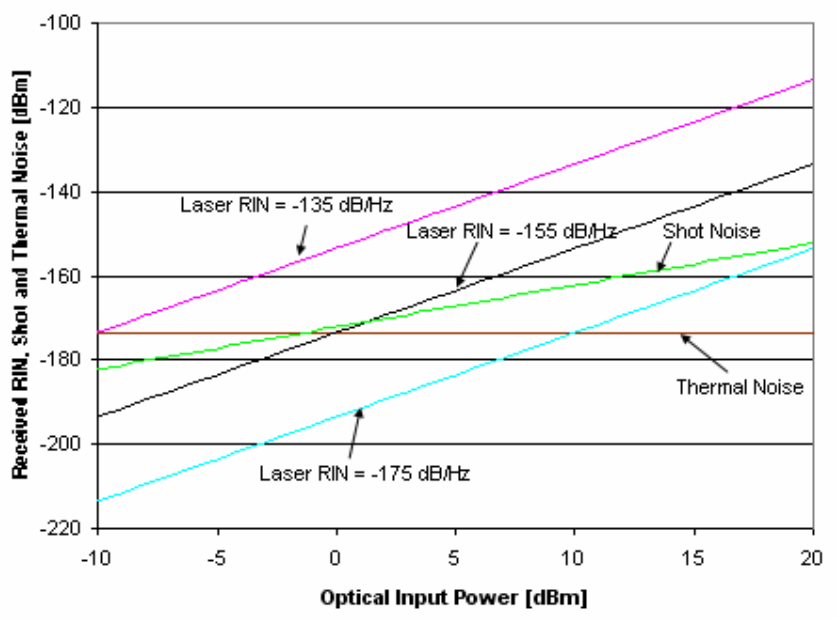


Figure 6. Received RIN vs. optical input power of the photodetector at different laser RIN.

Comparing with the shot noise, $\overline{i_{RIND}^2}$ is proportional to $\overline{I_D^2}$, whereas the shot noise is linearly proportional to $I_D$. Therefore, the *RIN* noise will tend to be the dominant noise, when the laser average power is increasing (see the

calculated curves in Figure 6). From Figure 5, we know that the received RIN noise for the single photodetector (S-PD) will be dominant, when the received optical power is greater than 2 dBm and thus, reduce the S/N ratio of the link.

The received RIN noise is very dependent on the RIN noise characteristics of the laser source. DFB lasers with RIN noise less than –170 dB/Hz have been developed and are now available as COTS devices. Figure 6 shows the received RIN of the photodiode vs. optical input power curves at different laser RINs. From this figure, we observe that for a laser having –175 dB/Hz RIN noise, the photodiode is shot noise limited almost up to 20 dBm optical input power.

The balanced photodetector (B-PD) will cancel the RIN noise in an analog link, even when the optical input powers of two photodiodes are mismatched as shown in Figure 7. However, for maximum RIN noise cancellation, it is recommended that the mismatch between two channels not exceed 5%.

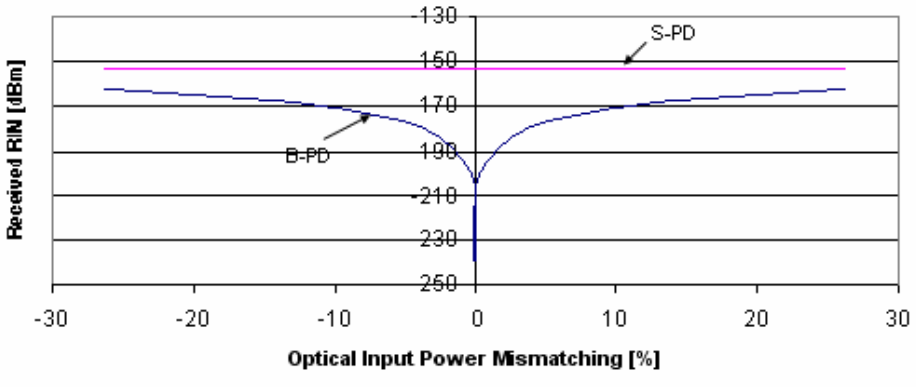


Figure 7. Optical input power mismatching effect on received RIN cancellation, here assume responsivity of the photodetector is 0.75 A/W, RIN of the DFB laser -155 dB/Hz, and optical input power of 10 dBm.

**3.2 SNR Improvement using Balanced Detection**

Assuming that all of the noise sources are uncorrelated, the signal-noise ratio of the link at the single photodetector can be expressed by:

$$SNR_S = \frac{i_D^2 \cdot \eta^2}{(\overline{i_{th}^2} + \overline{i_{sh}^2} + \overline{i_{RIN}^2}) \cdot \Delta f} \tag{5}$$

where, $\eta$ is the insertion loss (or gain) of the link. RIN noise contribution, being from the same source, is cancelled at the balanced receiver, while shot noise and thermal noise generated by the modulator driving circuit and receiver still remain factors in the total noise output power. The signal-noise ratio of the link at B- photodetector will be expressed by:

$$SNR_B = \frac{i_D^2 \cdot \eta^2}{(\overline{i_{th}^2} + \overline{i_{sh}^2}) \cdot \Delta f} \tag{6}$$

The improvement of the signal to noise ratio for the B-photodetector can be expressed as following equation:

$$\frac{SNR_B}{SNR_S} = \frac{(\overline{i_{th}^2} + \overline{i_{sh}^2} + \overline{i_{RIN}^2})}{(\overline{i_{th}^2} + \overline{i_{sh}^2})} = \frac{4kT_a / R + 2 \cdot e \cdot (I_d + \overline{I_D}) + RIN \cdot \overline{I_D^2}}{4kT_a / R + 2 \cdot e \cdot (I_d + \overline{I_D})} \tag{7}$$

Using $\overline{I_D} = \Re \cdot P_O$, above equation can be expressed as:

$$\frac{SNR_B}{SNR_S} = \frac{4kT_a / R + 2 \cdot e \cdot (I_d + P_O \cdot \Re \cdot \eta) + RIN \cdot (I_d + P_O \cdot \Re \cdot \eta)^2}{4kT_a / R + 2 \cdot e \cdot (I_d + P_O \cdot \Re \cdot \eta)} \tag{8}$$

Figure 8 shows the calculated results for SNR improvement of the B-PD in an analog photonic link at different laser RINs. It shows higher the RIN in a laser, the higher is the SNR improvement using a balanced photoreceiver.

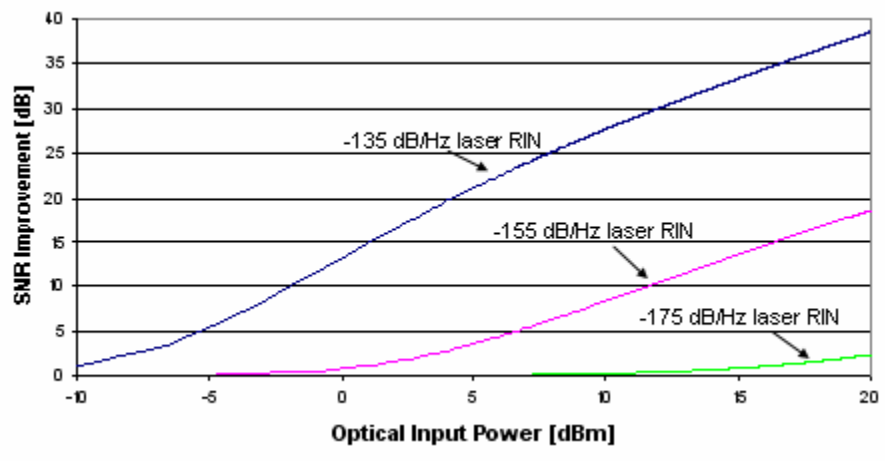


Figure 8. The SNR improvement of the B-PD at different optical input powers and different laser RIN.

**3.3 SFDR3 improvement using Balanced Detection**

The SFDR3 for a single photodetector analog photonic link can be calculated by the following equation [4]:

$$SFDR3 = \left(\frac{OIP3}{N_{out}}\right)^{2/3} = \left(\frac{8V_\pi^2}{kT_a \Delta f \cdot NF_S \cdot \pi^2 \cdot R_L}\right)^{2/3} \tag{9}$$

where, $OIP3$ is the RF output power of the 3rd intercept point, $N_{out}$ is output noise, and $NF_S$ is the noise figure of the S-PD link, & it can be obtained by following equation:

$$NF_S = \frac{(N_{thMO} + N_{RIND} + N_{ShotD} + N_{thD})}{G_{Link} \cdot N_{thMI}} \tag{10}$$

In B-photoreceiver, the received RIN having been canceled, the noise figure can be expressed as:

$$NF_B = \frac{(N_{thMO} + N_{ShotD} + N_{thD})}{G_{Link} \cdot N_{thMI}} \tag{11}$$

Using equations 9, 10, and 11, we can obtain the improvement of the SFDR3 for the B-Photoreceiver as follows:

$$\frac{SFDR3_B}{SFDR3_S} = \left(\frac{NF_S}{NF_B}\right)^{2/3} = \left[\frac{(N_{thMO} + N_{RIND} + N_{ShotD} + N_{thD})}{(N_{thMO} + N_{ShotD} + N_{thD})}\right]^{2/3} \tag{12}$$

Figure 9 shows the calculated result for SFDR improvement of the B-PD in an analog photonic link at different optical input powers, and different laser RINs. From this figure, we see that the photodiode is still shot noise limited at -175

dB/Hz laser RIN and ~ 20 dBm optical input power. In such a scenario, there is less SFDR improvement in the B-PD analog link.

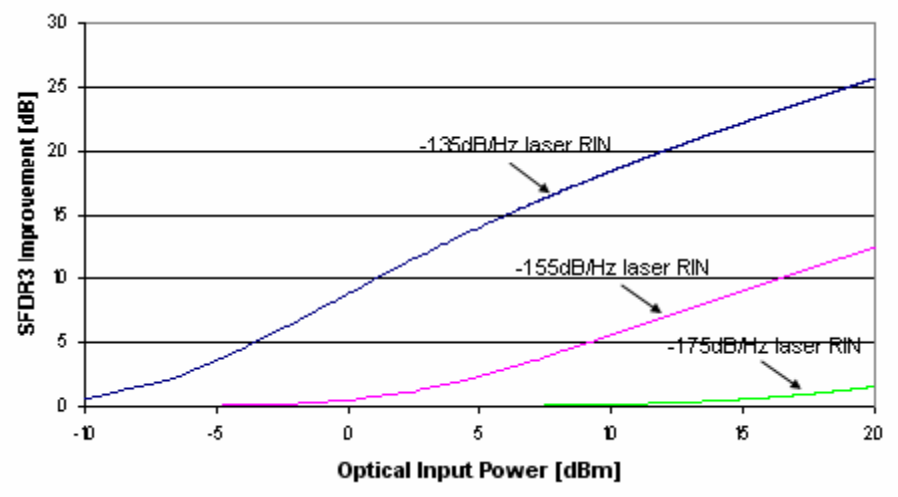


Figure 9. The SFDR improvement of the B-PD at different optical input powers and different laser RINs.

### 3.4 3rd Order Spurious Free Dynamic Range (SFDR3) Measurement

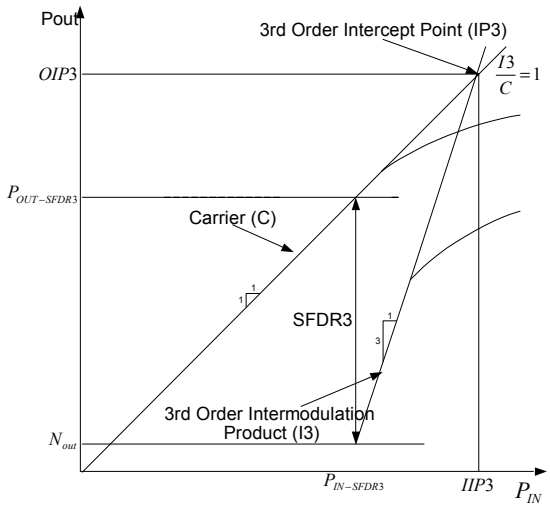


Figure 10. A plot illustrating the definition of spurious free dynamic range (SFDR) for analog photonic links.

The 3rd Order Spurious Free Dynamic Range (SFDR3) is illustrated in Figure 10. The intermodulation signals (carrier and 3rd order) generated from two equal tones can be measured experimentally. The Carrier (C) curve represents the variation in output power as function of input power for two fundamental input signals and the 3rd order curve depicts the behavior of the output power of 3rd order intermodulation product (I3) as a function of the fundamental input power. The intersection of two extended dashed line is the 3rd Order Intercept Point (IP3) & is obtained from this plot. The 3rd Order Spurious Free Dynamic Range (SFDR3) is defined as the difference between the output noise level ( $N_{out}$ ) and the output power point ( $P_{out-SFDR3}$ ) shown in the equation below:

$$SFDR3 = (P_{out-SFDR} - N_{out})\ \ dB \cdot Hz^{2/3} \qquad (13)$$

A two tone intermodulation distortion measurement was performed to obtain the spurious free dynamic range of the externally modulated photonic link with Discovery Semiconductors DSC720 balanced photodiode (B-PD) and DSC30S single photodiode (S-PD) at two tone carrier frequencies of $f1$=10 GHz and $f2$=10.001 GHz. Figure 11 shows results of two tone intermodulation distortion measurement showing the 3rd order spurious free dynamic range of the externally modulated analog photonic link using B-PD and S-PD. The average optical power coupled to the photodetector is 4.5 dBm for both B-PD and S-PD, and the output noise was measured in a 1 KHz bandwidth. The SFDR3 of the link for B-PD and S-PD is 85 $dB \cdot KHz^{2/3}$ ($105\,dB \cdot Hz^{2/3}$) and 83 $dB \cdot KHz^{2/3}$ ($103\,dB \cdot Hz^{2/3}$) respectively. The improvement of the SFDR3 for B-PD is $2\,dB \cdot Hz^{2/3}$ as compared with the S-PD for identical test conditions. It agrees with the calculated results shown in Figure 10 at about 5 dBm optical input power coupled to the photodiode and laser RIN of –155 dB/Hz.

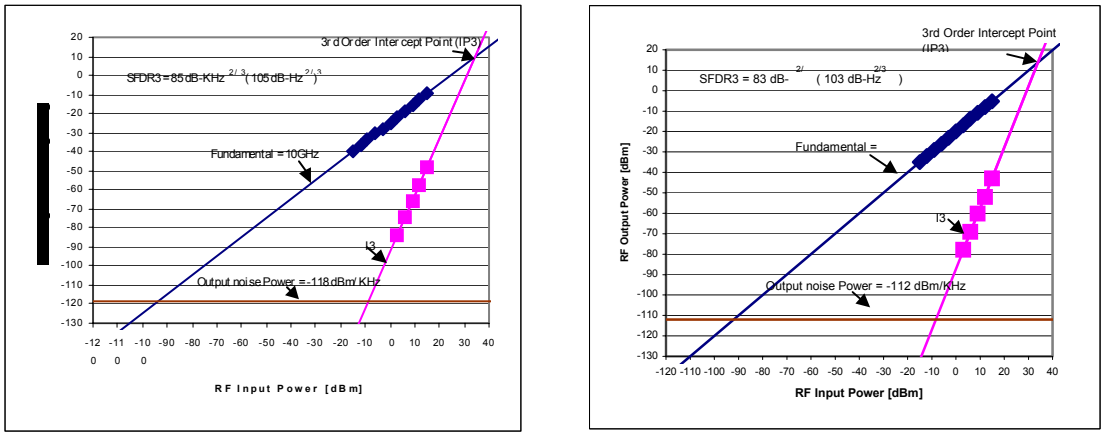


a) B-PD b) S-PD

Figure 11. Results of two tone intermodulation distortion measurement showing the 3rd order spurious free dynamic range of the externally modulated analog photonic link for B-PD and S-PD.

**3.5.Balanced Detection for digital DPSK and DQPSK modulation**

Recently there has been an increased interest in balanced detection for long-haul fiber optical transmission. This is due to the potential advantages of differential phase shift keying (DPSK) modulation techniques compared to conventional IM-DD. In the following sections, results using Discovery's balanced receiver R405 are summarized [5, 6]. In section 3.6, it is shown that the balanced receiver allows to increase the sensitivity by 3dB. In section 3.7, the increased performance achievable with balanced detection is demonstrated in a high capacity transmission experiment.

**3.6 Optically pre-amplified receiver sensitivities of 10Gb/s RZ-DPSK and 20Gb/s RZ-DQPSK**

To measure the receiver sensitivity of binary and quaternary differential phase shift keying (DPSK and DQPSK, respectively) the setup according to Figure 12 was implemented. The transmitter consisted of an external cavity laser (ECL) operating at a wavelength of 1539.75nm followed by two $LiNbO_3$ Mach-Zehnder modulators (MZM) that were operated in push-pull mode. The first MZM was driven with the 10 GHz clock signal to generate the RZ-pulse train. This was done by biasing the modulator at quadrature. The second MZM was used to form a phase-shift keyed signal. This MZM was biased at minimum. It was driven with a 10Gb/s non-return-to-zero (NRZ) electrical pseudo random bit sequence (PRBS) of length $2^9$-1. This sequence is referred to as $d_R$ because it forms the real part of the RZ-DQPSK signal.

The subsequent phase modulator (PM) consisted of a single $LiNbO_3$ optical wave guide with one electrode. It was driven with the complementary PRBS signal as used for the second MZM. According to the PRBS signal $d_R$, this

sequence is referred to as $d_I$ because it forms the imaginary part of the RZ-DQPSK signal. The driving voltage of the PRBS signal was adjusted to achieve a phase shift of 90° for the high level at the electrical input and 0° for the low level. An RF phase shifter was used to synchronize $d_R$ and $d_I$. It should be noted that the transit time for the optical signal from the second MZM to the PM was 10.5ns. This ensures that the two PRBS signals are uncorrelated.

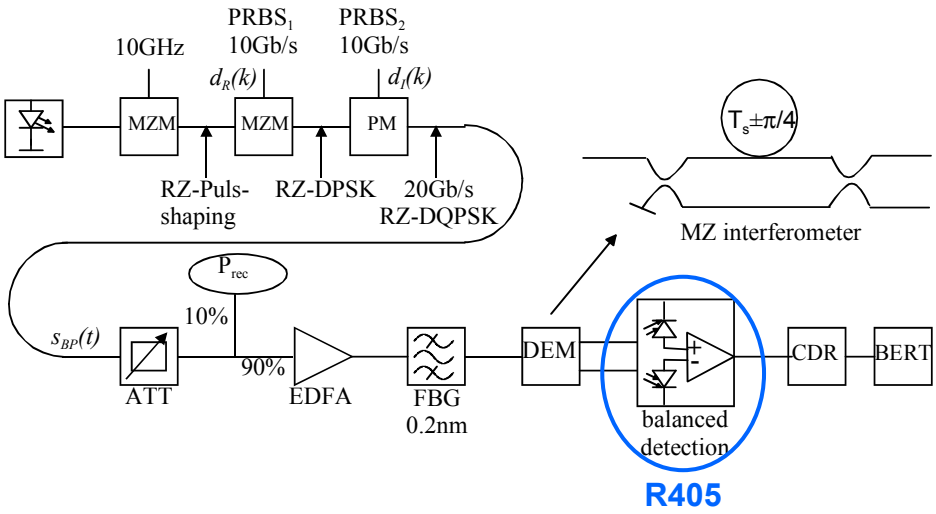


Figure 12. Experimental setup for RZ-DQPSK at 20Gb/s with autocorrelation detector.

An optical monitor coupler was used to measure the power of the transmitted signal before entering the 2-stage preamplifier. The small-signal gain and the noise figure of the erbium-doped fiber amplifier (EDFA) were 32dB and 4.5dB, respectively. Two external optical isolators (insertion loss: 0.2dB each) were placed in front of the preamplifier. After amplifying the signal it was filtered by a fiber bragg grating (FBG) with a center frequency of 1539.75nm and a bandwidth of 0.2nm to suppress the out-of-band ASE noise.

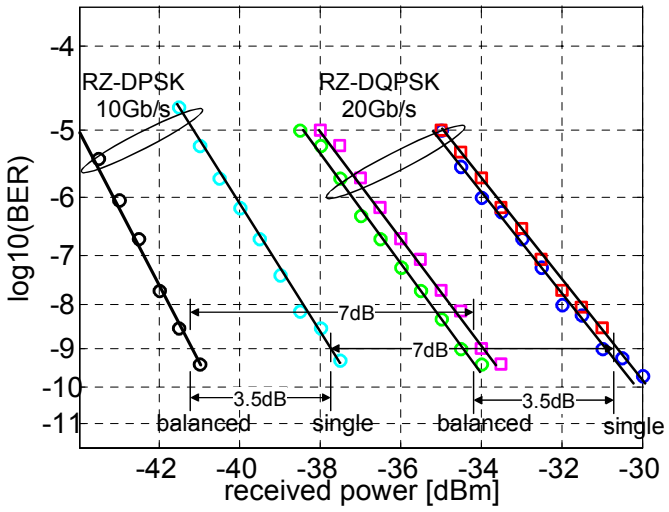


Figure 13. Measured BER values for RZ-DPSK format at 10Gb/s and RZ-DQPSK at 20Gb/s (real (○) and imaginary (□) component) for balanced (with R405) and single ended-detection, respectively.

The real (in-phase) and imaginary (quadrature) part of the DQPSK signal were detected by a Mach-Zehnder interferometer (MZI) that incorporated a delay of one symbol duration of 100ps (autocorrelation detector). It was based on two spliced fiber couplers. The phase difference between the signal and its delayed replica was adjusted thoroughly via temperature control of the length of the arms of the MZI. To detect the real and imaginary component of the DQPSK signal, the phase difference of the two band-pass signals has to be adjusted to +45° and –45°, respectively. In this way both components were measured separately on a data rate of 10 Gb/s per tributary. It is worth noting that this MZI is the same that is used for detecting binary DPSK signals. The two outputs from the MZI were fed to Discovery's low-noise balanced receiver R405 with a bandwidth of 14 GHz. The optical path lengths to the balanced receiver were roughly guaranteed by an appropriate splicing. In case of single-ended detection only one output of the MZI was used and connected to a standard photo diode with 12 GHz bandwidth. After clock- and data recovery (CDR) the BER was measured.

To measure the performance of binary RZ-DPSK format a similar setup as in Figure 12 was used. For generating the RZ-DPSK signal, the subsequent phase modulator was omitted. Moreover, the phase difference in the receiver-MZI was adjusted to 0°. Note that the transmission bit rate for DQPSK is 20Gb/s whereas for DPSK it is 10Gb/s. Figure 13 shows the measured BER values for RZ-DQPSK and RZ-DPSK for both single ended and balanced reception, respectively. The measured eye diagrams for the imaginary channel of RZ-DQPSK single ended and balanced detection are given in Figure 14. To measure these eye diagrams the received power at the preamplifier was set to –10dBm to reduce the noise sufficiently.

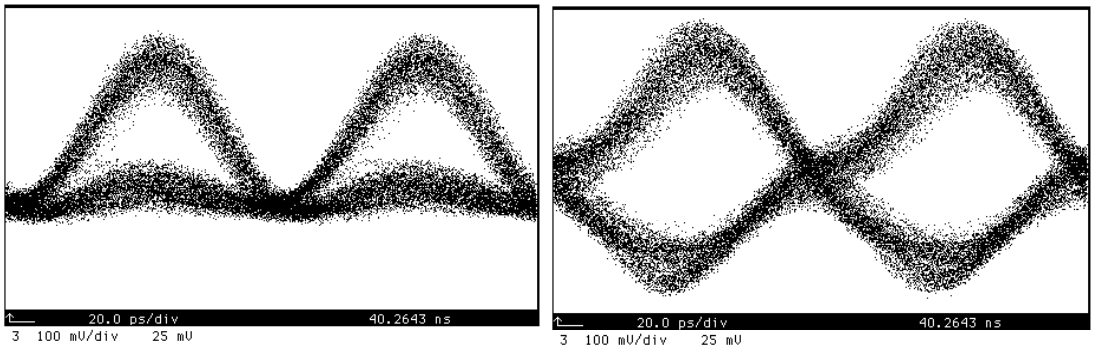


Figure 14. Measured eye diagrams for imaginary channel of RZ-DQPSK at 20Gb/s for single ended detection (left) and balanced (right, detected with DSC R405).

The BER-curves given in Figure 13 show that both for RZ-DPSK and RZ-DQPSK transmission the balanced detector performs 3.5dB better compared to the single-ended detector. 0.5dB are attributed to the better thermal noise properties of the balanced detector, which is confirmed by the fact, that for high BERs where the thermal noise is completely negligible compared to the ASE noise, there is only a difference of 3dB. This is known to be equal to the maximum performance improvement achievable for balanced detection with sufficiently narrowband filtering in front of the MZI.

**3.7 Highly efficient DWDM transmission with RZ-DQPSK**

To show the performance of a highly efficient transmission with balanced detection, the setup shown in Figure 15 was implemented. Output from eight distributed feedback lasers (DFB) with carrier frequencies from 192.375THz to 192.550THz with a 25GHz grid were multiplexed by a 8:1 star coupler. The laser outputs were simultaneously modulated with 20Gb/s RZ-DQPSK as described in Figure 12.

After RZ-DQPSK modulation the wavelength channels were polarization multiplexed so that each wavelength channel was comprised of two orthogonal polarization signals. A 10 kHz phase modulation was added to one of the signals which was used for polarization control at the receiver. The WDM signal was transmitted over two spans. Each span consisted of 100km of SSMF fully compensated by DCF. The average fiber input power for SSMF and DCF were 11dBm and 1dBm, respectively.

At the receiver side, the WDM signal was amplified and wavelength demultiplexed by a 25 GHz deinterleaver followed by a 50 GHz deinterleaver and a 100 GHz standard dielectric filter demultiplexer. After wavelength demultiplexing, polarization demultiplexing was performed. For sensitivity measurements, a variable optical attenuator in conjunction with an optical tap coupler was used to measure the power of the transmitted signal before entering the two-stage preamplifier. After amplifying, the signal was filtered by a tunable filter with a bandwidth of 0.2nm to suppress the out-of-band ASE noise. The real (in-phase) and imaginary (quadrature) part of the DQPSK signal were detected by a Mach-Zehnder interferometer (MZI) as described in Figure 12. Both components were measured separately at a data rate of 10Gb/s per tributary. The outputs from the MZI were fed to Discovery's R405 balanced receiver. The optical path lengths to the balanced receiver were guaranteed via variable optical delay lines. After clock- and data recovery (CDR), the bit error rate (BER) was measured.

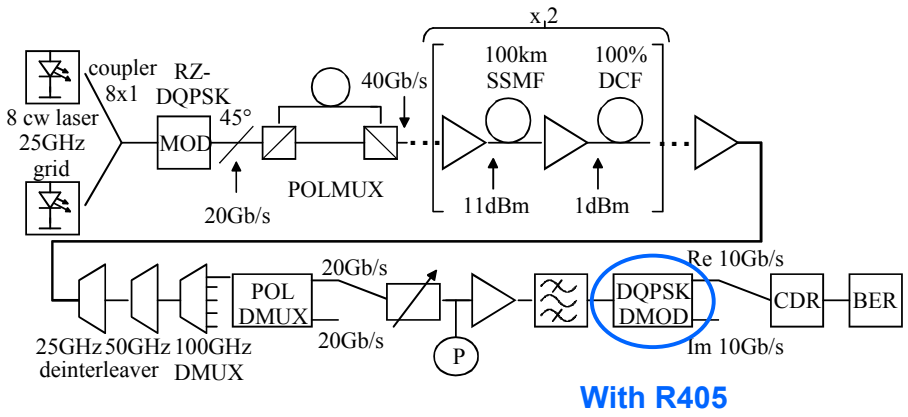


Figure 15. Experimental setup of 4x10Gb/s with 8 wavelengths over 200km SSMF and the eye diagrams before and after CDR module.

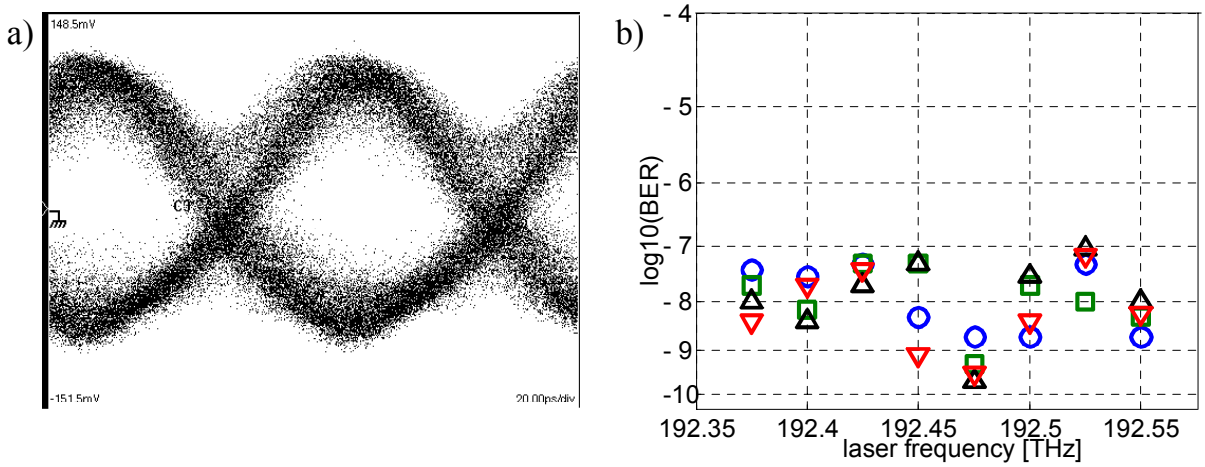


Figure 16: 4x10Gb/s with 8 wavelengths at 25GHz grid over 200km: a) Measured 10Gb/s eye diagram with R405, b) Measured BER values (uncorrected) for 8 wavelengths (4 tributaries each)

The WDM signal was transmitted over 200km. For each wavelength, the BER of each of the four tributaries was measured. The results are depicted in Figure 16b. BERs between $2x10^{-10}$ to $9x10^{-8}$ were measured. If standard forward error correction is applied, we expect error free transmission.

## 4. CONCLUSIONS

20 mA or higher photocurrent handling InGaAs photodiodes with 20 GHz bandwidth, and 10 mA or higher photocurrent handling InGaAs photodiodes with >40 GHz bandwidth have been developed. Theoretical calculation and experimental measurements indicate that the balanced photodiodes have several advantages as shown below:

1) The higher power handling B-PD cancels the RIN, thus, allowing increased optical power for higher SFDR;
2) Compared with a S-PD, the power handling of the B-PD is doubled;
3) The even order harmonics are canceled;
4) Reliability of a B-PD is increased because optical power is halved on each photodiode.

For digital applications, balanced detection of DPSK and DQPSK allows to increase the sensitivity by 3dB. Moreover, balanced detection of DPSK and DQPSK enables highly efficient digital fiber optic transmission which cannot be achieved with conventional IM-DD.

## 5. REFFERENCES


1. C. Cox and W. S. C. Chang, *Chapter 1: Figures of merit and performance analysis of photonic microwave links*, RF Photonic Technology in Optical Fiber Links, Edited by William S. C. Chang, 2002.
2. A. M. Joshi and X. Wang, *DC to 50 GHz Wide Bandwidth InGaAs Photodiodes and Photoreceivers*, Proc. SPIE, CR73, p. 181, 1999.
3. Hewlett-Packard Co, *Fiber Optic Test and Measurement*, Edited by Dennis Derickson, p. 272.
4. A. M. Joshi, *Dynamic Range Analysis for the Photonic Time Delay Unit*, Discovery Semiconductors Inc. Technical Report to Georgia Tech., 2003.
5. Wree, C., et al.: "Experimental Investigation of Receiver Sensitivity of RZ-DQPSK Modulation Format Using Balanced Detection", paper ThE5, Optical Fiber Communication Conference (OFC 2003), March 23-28, 2003, Atlanta, USA
6. Wree, C., et al.: "High spectral efficiency 1.6b/s/Hz transmission (8x40Gb/s with a 25GHz grid) over 200km SSMF using RZ-DQPSK and polarization multiplexing", IEEE Photonics Technology Letters, September 2003, Vol. 15, No. 93, pp. 1303-1305